Carbon-rich icy moons and dwarf planets

Bruno Reynard, Christophe Sotin

Earth and Planetary Science Letters 612 (2023) 118172

Contents lists available at ScienceDirect

Earth and Planetary Science Letters

journal homepage: www.elsevier.com/locate/epsl

Carbon-rich icy moons and dwarf planets

Bruno Reynard [a,*], Christophe Sotin [b]

[a] Univ Lyon, ENS Lyon, UCB Lyon 1, Univ St-Etienne, CNRS, Laboratoire de Géologie de Lyon, 69007 Lyon, France
[b] Laboratoire de Planétologie et Géosciences, Nantes Université, Univ Angers, Le Mans Université, CNRS, UMR 6112, F-44000 Nantes, France

ARTICLE INFO

Article history:
Received 9 November 2022
Received in revised form 24 February 2023
Accepted 14 April 2023
Available online 26 April 2023
Editor: J. Badro

Keywords:
icy moon
dwarf planet
carbonaceous matter
composition
differentiation
thermal evolution

ABSTRACT

Density and moment of inertia of icy moons and dwarf planets suggest the presence of a low-density carbonaceous component in their rocky cores. This hypothesis was tested using inner density structure and thermal models. Rocky core densities in dwarf planets and icy moons are found to consist of a mixture of chondritic silicate-sulfide rocks and carbonaceous matter. Carbonaceous matter was originally mixed with ice in a rock-free precursor. In a homogeneous accretion scenario where these components are mixed in solar proportions, ices then differentiated from the carbon-rich refractory core, while hydration of silicates could take place. Thermal models taking into account the presence of carbonaceous matter suggest that originally hydrated silicates are only partially dehydrated in the refractory cores of most moons. Viable scenarios point to a difference in formation or evolution between Ganymede and Titan in spite of their similar size and mass. Fully dehydrated mineralogies, inferred in Europa and possibly the densest dwarf planet Eris, require heterogeneous accretion near the water snow line of the solar or circumplanetary nebula. Progressive gas release from slowly warming carbonaceous matter-rich cores may sustain up to present-day the replenishment of ice-oceanic layers in organics and volatiles. It accounts for the observation of nitrogen, light hydrocarbons and complex organic molecules at the surface, in the atmospheres, or in plumes emanating from moons and dwarf planets. The formation of large carbon-rich bodies in the outer solar system suggests that carbon-rich planets could form at the outskirts of extrasolar systems.

1. Introduction

During its thirteen-year exploration of Saturn's environment, the Cassini mission returned precise gravitational data, which constrained the internal density structure of Titan, Enceladus, and Dione. Whatever the size of the moon, they are formed by rocky cores with a narrow range of densities of 2300–2500 kg/m^3, surrounded by thick ice-water mantles (Hemingway et al., 2018; Iess et al., 2012; McKinnon, 2015; Zannoni et al., 2020). Although not currently in the Outer solar System, Ceres may have formed at great heliocentric distance (De Sanctis et al., 2015). Internal structure models based on measurements by the Dawn mission point to a core whose density is similar that of Saturn's moons, surrounded by an ice-rich mantle (Ermakov et al., 2017; Mao and McKinnon, 2018).

As core densities are much lower than those of most chondritic rocks, an appropriate mineralogical and compositional model must be built. Densities of serpentine gives satisfactory results (Fortes, 2012) but only with Mg-rich composition that is difficult to reconcile with Fe-rich chondrite-like material in the outer solar system (Néri et al., 2020). Adding low density ice was proposed to explain low core density in a large body like Titan (Iess et al., 2012), but this solution is not satisfactory because geodynamical models demonstrated that ice melting and differentiation cannot be prevented (O'Rourke and Stevenson, 2014), separating liquids migrating upwards to form the hydrosphere from refractory compounds that formed the core. While porosity could help reducing core density in Enceladus core, it is unrealistic in bodies of the size or larger than Ceres where compaction is expected due to pressure.

Carbon in the form of organic matter is a major component of potential precursors of outer solar system bodies, namely carbonaceous chondrites with atomic C/Si up to ~0.8 (Lodders, 2003), comets with C/Si > 15 (Bardyn et al., 2017; Jessberger et al., 1988), Ryugu (Yokoyama et al., 2022) and dark asteroids (Martins et al., 2020). It was observed as complex organic molecules beyond the snow line of young extrasolar nebula (Lee et al., 2019). Carbonaceous compounds could exist beyond a "soot line" similar to the "snow line" and closer to the Sun (Kress et al., 2010), raising the possibility of forming C-rich water-poor planets (Lodders, 2004),

* Corresponding author.
E-mail address: bruno.reynard@ens-lyon.fr (B. Reynard).

https://doi.org/10.1016/j.epsl.2023.118172

and moons if a similar zoning existed in circumplanetary nebulae. Modeling the mineralogy of the refractory cores of the large icy moons Titan and Ganymede implies that 15–30 wt% of carbonaceous matter (COM) derived from chondritic insoluble organic matter (IOM) are buried in their interiors (Néri et al., 2020), and similar amounts were inferred for dwarf planet Ceres (Zolotov, 2020). Consequences of carbon-rich composition on core thermal evolution were however not investigated.

With growing evidence that large amounts of COM are present in icy moons and dwarf planets, we investigate compositional trends among these bodies using mineralogical models and explore consequences on their thermal evolution. Moment of inertia (MoI) is known for seven icy bodies: Ganymede, Europa, Titan, Enceladus, Dione, Haumea, and Ceres. For Haumea, the MoI is inferred from measurements of its triaxial ellipsoid shape. For the six other bodies, the MoI was deduced from gravity measurements. The MoI provides a strong constraint on the value of the core density assuming that a nearly pure water hydrosphere differentiated from the refractory core. We build compositional and thermal models consistent with these densities and discuss the consequences of the inferred high carbon contents on thermal evolution and formation scenarios.

2. Methods

2.1. Density calculations

A first component forms the icy layers and ocean. This icy component (IC) is assumed to be pure H_2O, allowing using well-known equations of state of H_2O when calculating the mass and MoI of the different bodies. It is likely that the ocean is salty as demonstrated by the presence of an induced magnetic field on Europa and Ganymede. However, the amount of salt and its nature is difficult to constrain from available data (Vance et al., 2014).

The density of the refractory core is calculated from the densities of two components: the silicates and sulfides component (SSC) and the carbonaceous organic matter (COM).

SSC composition (Table S1) is taken as the non-carbonaceous fraction of a simplified CI carbonaceous chondrite composition (Néri et al., 2020). SSC densities at ambient conditions take values of ∼3150 kg/m^3 and ∼3750 kg/m^3 for the fully hydrated and the dry mineralogy, respectively, calculated using the Perple_X code (Connolly, 1990). Density and normative mineralogical calculations can be reproduced at ambient conditions with the material provided in supplementary information (Excel spreadsheet dataset S1). At first order, density varies with the total water content of the SSC, and increases with temperature as silicates dehydrate. If the core is hot enough, a liquid inner metallic core segregates from an iron-depleted silicate mantle. With the slow radioactive warming (section 3.3), equilibrium should be reached at eutectic temperature (∼1200 K) and composition (Fei et al., 1997), giving metal and silicate mantle densities of 5700 kg/m^3 and 3200 kg/m^3, respectively (Néri et al., 2020). Ganymede's internal dynamo requires an at least partly differentiated core (Kivelson et al., 2002), and it is also possible in Europa. It has a bulk-decompressed density of ∼3800 kg/m^3, marginally higher than the value of 3750 kg/m^3 for the dry undifferentiated SSC, thus the later value was used. Typical uncertainty on density of SSC is 2%.

COM, the second refractory component, is made of carbonaceous matter derived from chondritic refractory organic matter or IOM. It transforms irreversibly upon heating by loosing heteroatoms (Okumura and Mimura, 2011), ultimately transforming into carbon. In the absence of data for IOM and COM, density is estimated to be similar to that of terrestrial coals of 1400 ± 200 kg/m^3. Density of coals is constant up to heating temperatures of 673 K (Franklin, 1949), close to the dehydration temperature of the abundant hydrated silicate serpentine (Néri et al., 2020). Coal density increases to 1800 ± 200 kg/m^3 on heating to 973 K (Franklin, 1949), a value used for modeling Ganymede (Néri et al., 2020), and gradually reaches that of graphite (∼2300 kg/m^3) at higher temperatures like those attained in Europa. A large uncertainty of ±200 kg/m^3 is assigned to account for compositional variability of COM in meteorites and IDP (Dartois et al., 2013) and for unknown effects of compressibility and thermal expansivity. In a first step, COM is assumed to consist of pure C, an assumption that is released in a second step (see section 3.2) because heteroatom concentration decreases on heating (Franklin, 1949; Okumura and Mimura, 2011), leading to a potential loss to volatiles (CH_4, CO, CO_2, hydrocarbons) of about 40% in mass between 700 and 1200 K. Volatile carbon species are assumed to escape to the hydrosphere or atmosphere along with silicate dehydration fluids. Contribution of carbonates, minor components of carbonaceous chondrites, is neglected in the present model.

Densities of mixtures are calculated from volume conservation on mixing:

$$\rho_{mix} = \frac{\rho_1 \rho_2}{\rho_1 (1 - X_1) + \rho_2 X_1} \quad (1)$$

with ρ_{mix} the density of the mixture, ρ_1 and ρ_2 the density of components 1 and 2, X_1 the mass fraction of component 1. Densities calculated for carbonaceous chondrite compositions including both the SSC and COM components (Lodders, 2003; Wasson and Kallemeyn, 1988) compare well with grain densities of carbonaceous chondrites (Macke et al., 2011) of different metamorphic grades (Fig. S1). CM2 meteorites have densities comparable to fully hydrated, CO3 to partially hydrated, CO3-4 and CV3 to dry silicate mineralogies. On the parent body of CV carbonaceous chondrites, metamorphic temperatures in the 473–883 K range are inferred for CV3 type (Ganino and Libourel, 2017). Thus reactions that occurred within the short-lived (>10 Ma) parent body metamorphism had enough time to take place in larger bodies where metamorphism lasts much longer (Castillo-Rogez and Lunine, 2010). Experiments also suggest geologically rapid alteration of silicates even close to the melting point of ice (Zandanel et al., 2022), justifying the assumption of thermodynamic equilibrium in the Perple_X model. Effects of compression and thermal expansion on densities are small with respect to compositional effects, and to the large uncertainties on COM density, even in Ganymede and Titan where maximum pressures of ∼5 GPa are reached. This is supported by the fact that similar amounts of COM are found for Titan and Ganymede in the present study (see section 3.1) and when taking explicitly into account equations of state (Néri et al., 2020).

Density was calculated for a solar composition with C/Si = 7.08 and O/Si = 14.13 (Lodders, 2003). O is partially consumed to oxidize other elements/compounds except FeS and C to form silicates and oxides. The remaining O along with H forming H_2O ice, are added up to match the solar ratios, and form the icy component (IC). The density of this solar mixture is 1480 ± 70 kg/m^3 at ambient conditions, where the refractory core (71 SSC + 29 COM in wt%) has an ambient density of 2300 ± 130 kg/m^3 assuming a hydrated mineralogy mixed with low-density (1400 kg/m^3) COM. Bulk solar density becomes 1580 ± 50 kg/m^3 and core density is 3150 ± 70 kg/m^3 assuming a dry mineralogy mixed with graphite density (2300 kg/m^3) COM. For hydrated cores, water is partitioned between IC and SSC that contains ∼9 wt% H_2O, thus we define isochemical components IC* = IC + 0.09 SSC and SSC* = 0.91 SSC (for dry cores, IC* = IC and SSC* = SSC). Solar composition is 41 wt% of IC*, 19 wt% of COM (assumed to be pure C), and 40 wt% of dry SSC* (Fig. 1). Uncertainties on densities include chemical variability of CI chondrites (Lodders, 2003), and depend largely on the

carbon content because of the large assumed uncertainties on COM density.

2.2. Thermal modeling

The temperature profile $T(t,r)$ in the refractory core of a spherical body is determined by solving the 1D conduction energy conservation equation in spherical coordinates:

$$\frac{\partial\left(k^{\partial T}/_{\partial r}\right)}{\partial r}+\frac{2}{r}\left(k^{\partial T}/_{\partial r}\right)=\rho C_P\left(\frac{\partial T}{\partial t}\right)-Q(r,t) \tag{2}$$

where t is time, r radial coordinate, k is thermal conductivity, ρ is density, C_P is specific heat, and $Q(t,r)$ is the volumetric heating rate. We use the analytical solution (Carslaw and Jaeger, 1959) established for a volumetric rate $Q(r,t)=Q_0e^{-\lambda t}$ of a sphere of radius R with constant temperature T_0 at $r=R$ and a uniform temperature T_0 at $t=0$:

$$T=T_0+\frac{\kappa Q_0}{k\lambda r}e^{-\lambda t}\left(R\frac{\sin\left(\sqrt{\frac{\lambda}{\kappa}}r\right)}{\sin\left(\sqrt{\frac{\lambda}{\kappa}}R\right)}-r\right)+\frac{2Q_0R^3}{k\pi^3 r}\sum_{n=1}^{\infty}\left[\frac{(-1)^n}{n\left(n^2-\frac{\lambda R^2}{\kappa\pi^2}\right)}\sin\left(\frac{n\pi r}{R}\right)\exp\left(-\frac{n^2\pi^2\kappa}{R^2}t\right)\right]. \tag{3}$$

Temperature T_0 is the melting temperature of ice since the differentiation of the hydrosphere happens quickly once this temperature is achieved (O'Rourke and Stevenson, 2014). It is assumed constant.

The heating rate depends on the amount of each radioactive element i contained in the silicate fraction after differentiation and on the mass fraction of COM (X_{COM}):

$$Q(t)=\rho_{core}\sum_i H_{i,0}\left(1-y_{i,leaching}\right)(1-X_{\mathrm{COM}})\mathrm{e}^{-\lambda_i t}. \tag{4}$$

It was approximated by:

$$Q(t)=Q_0\mathrm{e}^{-\lambda t}=\rho_{core}H_0\left(1-y_{leaching}\right)(1-X_{\mathrm{COM}})\mathrm{e}^{-\lambda t}, \tag{5}$$

where the initial heating rate (H_0) and the effective decay constant (λ) are fitted to the curve obtained by summing the contributions of the four main long-lived radioactive elements (^{40}K, ^{232}Th, ^{235}U, ^{238}U) for different starting compositions (CV, CI, Bulk Solid Earth, see Table S2). Values for CI chondrites were used here. Heat production for CV and BSE compositions is similar to that obtained for CI rock with $y_{leaching}$ of ~0.23 and 0.38, respectively.

The coefficient $y_{leaching}$ represents the fraction of radioactive elements leached by dissolution during the differentiation process and is assumed to be the same for all radioactive elements. Chemical leaching may occur at low temperatures when water/ice and rocks interact prior to and during ice-core differentiation (Zandanel et al., 2022), and may proceed during porosity compaction and release of fluids over the broad dehydration window when temperature rises (Néri et al., 2020). We then defined a global leaching parameter that includes chemical leaching by dissolution during differentiation and the delay in the thermal evolution of the refractory core after full ice-core differentiation. Before and during ice-core differentiation, the temperature is buffered by the melting temperature of ice as the water migrating from the undifferentiated interior transports heat. Radioactive heating of the core thus starts after a delay in differentiation that can last up to several hundreds of million years (O'Rourke and Stevenson, 2014), and we have:

$$Q(t)=\rho_{core}H_0\left(1-y_{leaching}\right)(1-X_{\mathrm{COM}})\,\mathrm{e}^{-\lambda\left(t_{diff}+t^*\right)} \tag{6}$$

$$Leaching\ parameter=\left(1-y_{leaching}\right)\mathrm{e}^{-\lambda t_{diff}} \tag{7}$$

where t_{diff} is the time when differentiation is complete and t^* the time since differentiation ($t=t_{diff}+t^*$). With the value of $\lambda=5.05\ 10^{-4}$ My^{-1}, differentiation times of 100, 500 and 1000 Myr yield in 95, 78, and 60% of initial value of H_0 or leaching parameters of 0.05, 0.22 and 0.4, respectively. For bodies like Ganymede with at least a partly differentiated core, the growth of a metallic inner core redistributes the heat production and releases gravitational energy. Gravitational energy (<3.4 10^{28} J) is equivalent to about 350 Myr of radioactive decay. Although not negligible, these effects were not taken into account here because they are of second order (about 50 K increase of central temperature for gravitational energy) with respect to the effect of adding COM (about 400 K difference in final central temperature for 25% COM; Fig. S2). This will be addressed in specific models applied to Ganymede and Europa where time-dependent parameters are implemented.

Equation (6) provides an efficient way of investigating the effect of COM on the temperature evolution in the core as well as the effect of leaching during differentiation (Castillo-Rogez and Lunine, 2010). The parameters for equation (6) are calculated using the thermal characteristics of antigorite, magnetite, and iron-sulfide for SSC, and of coals for COM (Clauser and Huenges, 1995; Herrin and Deming, 1996; Osako et al., 2010). The values are calculated using volume average for thermal conductivity and mass average for specific heat, with mass fraction of COM varying from 0 to 50%. The value of thermal diffusivity ($\kappa=k/\rho C_P$) is calculated from the averaged values of thermal conductivity, density and specific heat (Table 1). Increasing COM content with low coal-like properties lowers thermal diffusivity, which would increase final temperatures, but this effect is counteracted the dilution of radioactive production by unit volume, resulting in lower final temperatures. The development of a model that self-consistently accounts for changes with temperature of density, thermal conductivity, specific heat and degree of graphitization is out of the scope of the present paper, as well as modeling migration of volatiles and compaction of the core with metamorphism.

Table 1
Parameters used in thermal models (bold) are calculated from values for the three listed minerals for the SSC component and for coals for the COM component.

	M (g/mol)	ρ (kg/m^3)	% wt	C_P (J/kg/K)	k (W/m/K)
$Mg_3Si_2O_5(OH)_4$	277.1	2580	64	1250	2.7
Fe_3O_4	231.55	5180	18	1100	4.6
FeS	87.91	4910	18	693	3.5
SSC		**3130**	**50–100**	**1124**	**2.98**
COM		**1400–1800**	**0–50**	**1500**	**0.2**

3. Results

3.1. Composition of icy moons and dwarf planets

Fractions of IC, COM and SSC in icy moons and dwarf planets were determined (Fig. 1) assuming a H_2O hydrosphere differentiated from a refractory core consisting only of SSC + COM to limit the possible range of density structures for a body of given MoI and mass (Table 2). The relative mass of the hydrosphere gives the IC fraction. Core densities determine the SCC and COM fraction (equation (1)) when density is fixed to 1400 kg/m^3 for COM and ~3150 kg/m^3 for the cold hydrated SSC cores in all bodies

Table 2
Physical characteristics and composition of icy satellites and dwarf planets, core densities are decompressed to ambient conditions (estimated uncertainty on last digits in parentheses).

Name	Density (kg/m^3)	Radius (km)	MoI	IC (wt%)	SSC (wt%)	COM (wt%)	COM in core (wt%)	Core density (kg/m^3)
Callisto	1834	2403.0						
Ganymede	1940	2634.0	0.311	35	48	17	26	3010(100)
Europa	2970	1561.0	0.347	8	73	19	21	3350(100)
Titan	1881	2575.0	0.3414	31	54	15	22	2490(100)
Rhea	1236	764.0						
Iapetus	1088	734.0						
Dione	1478	561.0	0.33	39	46	15	25	2400(300)
Tethys	984	531.0						
Enceladus	1641	252.0	0.33	31	54	15	22	2500(150)
Mimas	1230	198.0						
Triton	2061	1353.4						
Titania	1711	788.0						
Oberon	1630	761.0						
Umbriel	1390	585.0						
Ariel	1592	579.0						
Miranda	1200	236.0						
Ceres	2162	469.7	0.373	15	62	24	28	2420(100)
Pluto	1860	1188.3						
Charon	1586	606.0						
Eris	2520	1163.0						
Haumea	2018	780.0	0.282	23	63	14	18	2650(90)
2007 OR_{10}	1720	625.0						
Quaoar	1955	555.0						
Orcus	1560	459.0						
Salacia	1343	427.0						
Varda	1240	361.0						
2002 UX_{25}	869	325.0						

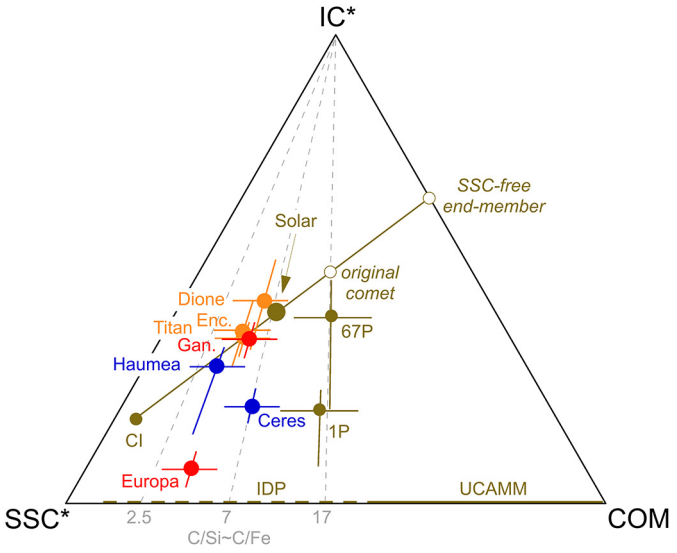

Fig. 1. Composition of icy moons and dwarf planets and potentials precursors in a ternary diagram (SSC*: dry silicate-sulfide, IC*: hydrosphere and water in silicates, COM: carbonaceous matter). Moons of giant planets are shown in red (Jupiter), orange (Saturn), and dwarf planets in blue. Component mass fractions for each body are inferred from mineralogical modeling of the inner density structure (Table 2). Precursors: solid brown symbols, comets (1P-67P) likely formed on the CI-solar continuum and lost ice by sublimation. Their original composition is given by the intersection of the CI-solar line and lines with constant elemental ratio C/Fe $\approx 17 \pm 2$ in 1P (Jessberger et al., 1988), equivalent to the COM/SSC ratio of 45/55 inferred in 67P (Bardyn et al., 2017). The ice/rock ratios are taken from Jessberger et al. (1988) for 1P and Rotundi et al. (2015) for 67P. IDP (dashed brown line) and UCAMM (full brown line) are assumed to be cometary grains having lost ice by sublimation and cover the whole range of C/Si ratios (Dartois et al., 2013) from CI to SSC-free end-member of the CI-solar continuum.

except Europa and Ganymede. For Europa and Ganymede, COM densities were chosen as 2300 and 1800, respectively, and a value of ~3750 kg/m^3 for a dry SSC core was used. Ranges of COM mass fraction are 18–32% for Ceres, 13–29% for Enceladus, 12–42% for Dione, 17–29% for Titan, 9–18% for Haumea, 18–28% for Ganymede, and 16–26% for Europa using core densities from modeling of the MoI of Ganymede, Europa, Titan, Enceladus and Dione (McKinnon, 2015; Néri et al., 2020; Sohl et al., 2002; Zannoni et al., 2020) for icy moons, Ceres and Haumea (Dunham et al., 2019; Ermakov et al., 2017) for dwarf planets (Table 2).

Compositions of Ganymede, Titan, Enceladus, Dione and Haumea plot close to the line that connects the CI and solar compositions (Fig. 1). These bodies can have formed by homogeneous accretion of SSC grains up to small carbonaceous chondrite-like parent bodies, and a mixture of ice and COM in proportion inferred from the projection of the CI-solar line towards an SSC-free end-member (~67 wt% IC and 33 wt% COM) before differentiation of the core. Although porosity may be present in Enceladus, porosity is not required for modeling its internal structure assuming a composition similar to that of larger Saturnian moons. Dwarf planets Ceres and Jupiter's moon Europa plot below the CI-solar line, requiring either a heterogeneous accretion that began out of the ice stability field in the protosolar or protoplanetary nebula, or ice loss subsequent to ice-core differentiation, hypotheses that are discussed later. All bodies are poorer in C (C/Si < 7) than the solar composition (C/Si ~ 7.1), Haumea being the most enriched in SSC. This can be partly attributed to C loss during differentiation and thermal processing of the original organic matter that was accreted to form these bodies as discussed in the next section. Haumea's depletion in volatile elements may also reflect formation partly ahead of the snow line.

3.2. COM metamorphism and temperature estimates

Alternatively to fixing COM density to arbitrary values, the mass fraction of COM can be fixed, and the corresponding density of COM required for matching the core density deduced (Fig. 2). As temperature increases, COM density increases and its mass fraction decreases due to extraction of soluble organic matter (SOM) during ice/core differentiation and of volatiles at higher temperatures. SOM accounts for less than 30% of the total organic matter (Piz-

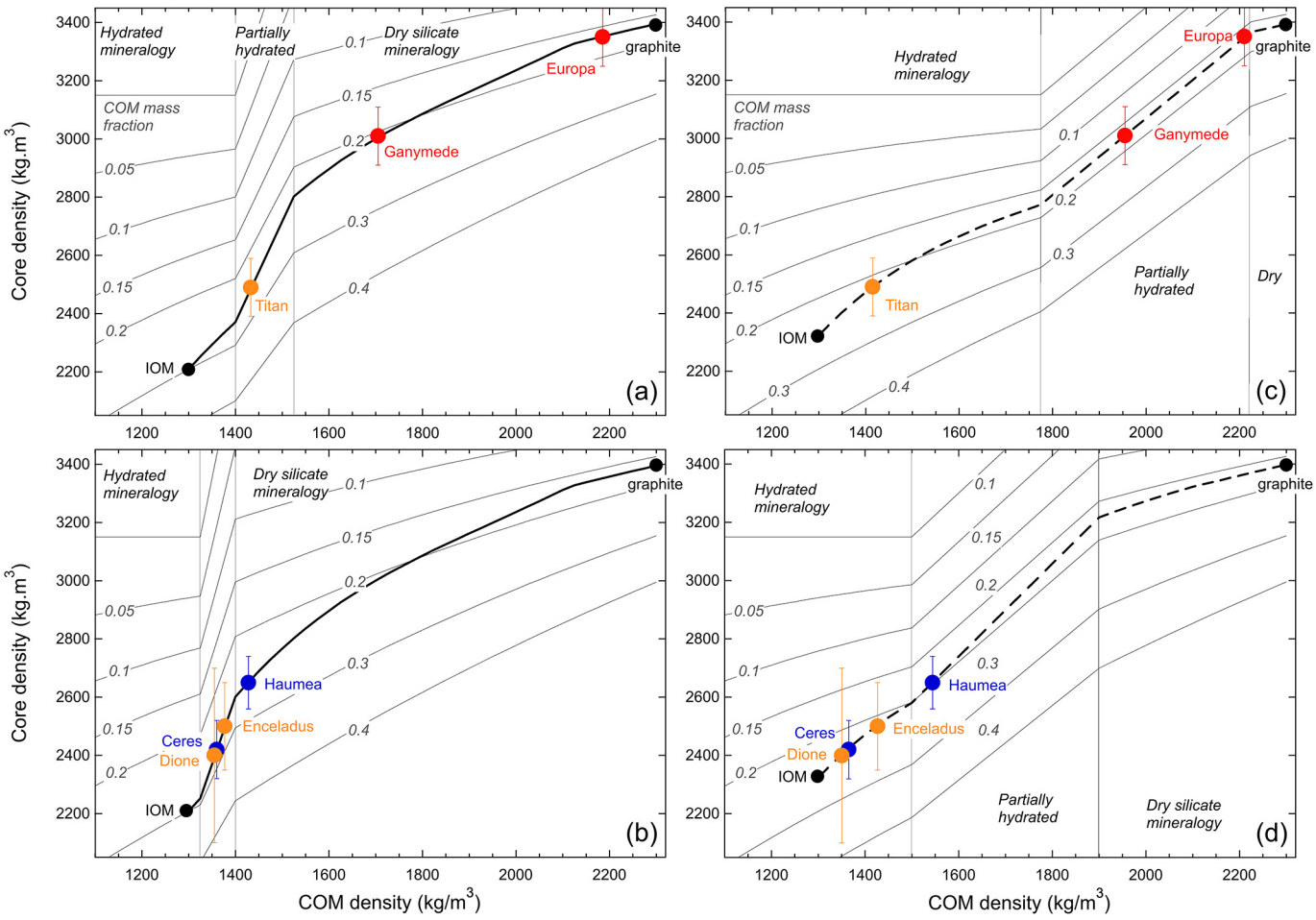

Fig. 2. Densities and proportions of COM (thick lines) inferred for (a) large bodies where pressure fixes the dehydration interval at ~593–853 K, and (b) small bodies where pressure fixes the dehydration interval at ~493–653 K. Densities of refractory core-forming mixtures (thin curves) are calculated for various mass fractions of COM and SSC in hydrated and dry core mineralogies of density ~3150 kg/m^3, and ~3750 kg/m^3, respectively. Evolution of the core density assumes a solar fraction of COM whose density and composition evolves as temperature increases according to pyrolysis experiments (thick curve). Decompressed densities of cores in seven bodies are reported to obtain the corresponding COM density and temperature window of metamorphism (Fig. 3). (c) and (d) same as (a) and (b) with COM density and composition calculated with the Vitrimat model (dashed thick curve). Dehydration windows are shifted to higher COM density because densification occurs at lower temperature than that inferred from pyrolysis experiments (see Fig. 3 and section 3.2). Note that differentiated cores of Ganymede and Europa with SSC density of up to 3800 kg/m^3 would increase the amount of COM by 1–2% (see section 2.1). For the sake of clarity, partially hydrated density is linearly interpolated between hydrated and dry densities. Same color code as Fig. 1.

zarello et al., 2006). It is composed of light organic molecules that can volatilize during formation or separate from the core with the ice during the initial differentiation, and we estimate a maximum value of 25% of the C mass is lost by this process. The remaining 75% of C (or 22% in total mass assuming initial solar composition) are contained in the so-called IOM (Alexander et al., 2007; Okumura and Mimura, 2011) that was processed at low temperature in CI carbonaceous chondrite material such as that sampled on asteroid Ryugu (Yokoyama et al., 2022).

There is a lack of data on the transformation kinetics and densification of IOM at high temperature and pressure relevant planetary interiors, which should be filled by future experiments. The evolution of IOM composition with temperature was determined from pyrolysis experiments (Okumura and Mimura, 2011) performed over short heating steps (10 minutes) when maturation of organic matter occurs over geological timescales. On the other hand, kinetic models of maturation and densification of coals at geological heating rates (Burnham, 2019), and density changes during coal pyrolysis (Franklin, 1949) have been determined. However, IOM belongs to non-graphitizing materials (Franklin and Randall, 1951) with incomplete transformation to graphite, while coals belong to graphitizing materials, making them debated analogs (Alexander et al., 2007).

In the absence of density and kinetic data on IOM, we define two extreme kinetic models. Firstly we use the pyrolysis data to simulate non-graphitizing IOM with delayed densification. Noting that coal density depends almost uniquely on its H/C atomic ratio, not its O/C ratio, we assume this remains valid up to oxygen concentration of IOM and COM, and estimate their density from the density-composition relation established for coals (Fig. S3). Secondly we assume that COM properties follow the evolution of coal density and composition over geological timescales given by the Vitrimat model (Burnham, 2019). The densification windows occur at higher temperatures for the first model than for the second (Fig. 3). The lower transformation temperatures in the Vitrimat model reflect the effects of kinetics over geological timescales.

Upon pyrolysis, volatiles and hydrocarbons are released (Okumura and Mimura, 2011), which allows writing a suite of irreversible reactions at each temperature step that sum up to:

$$C_{100}H_{65}O_{17}N_{3.5}S_2(\text{IOM}) \rightarrow 63C + 3H_2O + 27.5\text{“}CH_2\text{”} + 4.5CO_2 + 5CO + 2H_2S + 1.75N_2, \quad (8)$$

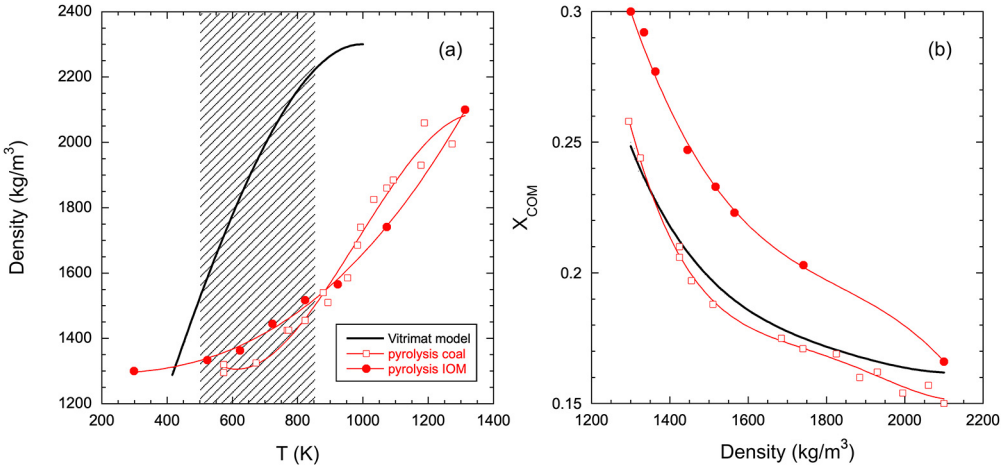

Fig. 3. Evolution of densities and proportions of COM for the pyrolysis and Vitrimat models. (a) model density of pyrolysed IOM increase smoothly with increasing temperature whereas that of coals in the Vitrimat model increase rapidly from 400 to 1000 K. Density of pyrolysed coals is also shown for illustrating the difference with Vitrimat due to kinetic effects. Metamorphic crystalline graphite formed at ~1000 K (Beyssac et al., 2002) fixes the high temperature limit for full densification to 2300 kg/m^3 for extrapolating the Vitrimat model. IOM pyrolysis model is used for simulating the evolution of "non-graphitizing" COM, and Vitrimat for coal-like graphitization. Shaded area indicates the silicate dehydration windows. (b) Evolution of the fraction of COM (X_{COM}) as a function of density starting from a solar composition at 1300 kg/m^3, computed from chemical reactions at each temperature increment. Data for pyrolysis of IOM (Okumura and Mimura, 2011) and coals (Franklin, 1949) were used, and results from Vitrimat (Burnham, 2019) setting a heating rate of 1 K/Myr.

where "CH_2" is a proxy for average composition of released hydrocarbons. The mass fraction of COM decreases with increasing density according to the stoichiometric factor at each reaction step (Fig. 3) and its relationship with density is fitted in the 300–1300 K range as:

$$X_{COM} = X_C \times m_{COM}/m_C = 0.3 - 4.3\,10^{-4}\,\Delta\rho + 6.6\,10^{-7}\,\Delta\rho^2 - 4.1\,10^{-10}\,\Delta\rho^3, \quad (9)$$

where X_{COM} is the mass fraction of organic matter, X_C is the mass fraction of carbon starting at 22% (see above), m_C its molar mass of 12, m_{COM} the molar mass of COM for one atom of carbon, $\Delta\rho = \rho_{COM} - 1300$ in kg/m^3, and ρ_{COM} is the density. Equation (9) is valid up to a density of 2100 kg/m^3 are assumed after which $X_{COM} = X_C$ is constant. Density evolution with temperature is fitted as (Fig. 3):

$$\rho_{COM} = 1314 - 0.16\,T + 2.8\,10^{-4}\,T^2 + 2.3\,10^{-7}\,T^3, \quad (10)$$

which is valid in the 573–1420 K range. Values of ρ_{COM} of 1300 and 2300 kg/m^3 are assumed below 573 K and above 1420 K, respectively.

Setting a heating rate of 1 K/My in the Vitrimat model, the predicted evolution of density and composition (Fig. 3) is used to obtain:

$$X_{COM} = 0.25 - 3.7\,10^{-4}\,\Delta\rho + 7.7\,10^{-7}\,\Delta\rho^2 - 8.4\,10^{-10}\,\Delta\rho^3 + 3.6\,10^{-13}\,\Delta\rho^4, \quad (11)$$

which is valid up to a density of 2100 kg/m^3 after which $X_{COM} = X_C$ is constant, and:

$$\rho_{COM} = 50 + 2.75\,T + 1.3\,10^{-3}\,T^2 - 1.8\,10^{-6}\,T^3, \quad (12)$$

which is valid in the 400–1000 K range. A value of ρ_{COM} of 2300 kg/m^3 is assumed above 1000 K.

Equations (9), (12) are used to calculate the evolution of core density at fixed solar COM fraction and comparing with the densities of the seven bodies of know MoI (Fig. 2). Temperature governs the density increase in both silicates through dehydration and carbonaceous matter through carbonization (Fig. 2). It is estimated from the COM density using equations (10) and (12), and fixes the position of the silicate dehydration window that occurs at ~493–653 K at low pressure for Haumea and smaller bodies, and at ~593–853 K at higher pressure for Europa and larger bodies.

With COM composition and density derived from pyrolysis (Fig. 2a,b), the core densities of Dione, Ceres, and Enceladus are compatible with hydrated to partially hydrated silicate mineralogies, that of Haumea with nearly totally dehydrated mineralogy, that of Titan with partially hydrated mineralogy and those of Ganymede and Europa with dry silicate mineralogy and COM density increasing towards that of graphite (~2300 kg/m^3). With COM composition and density derived from the Vitrimat model at geological heating rates (Fig. 2c,d), Haumea is marginally dehydrated, Ganymede is half dehydrated, Europa is essentially dry, all other bodies being consistent with fully hydrated silicate mineralogy. Volatile components released by COM densification are assumed to escape to the outer layers of the planetary body along with silicate dehydration fluids. As mentioned in section 2, potential C-bearing fluid interactions with rocks and ices were not taken into account, a simplification that should be dealt with in future models and tailored to specific bodies.

3.3. Thermal evolution

Maximum temperatures after 4.5 Gyr and volume fraction of the core that became hotter than dehydration temperatures were calculated for radii of 500 to 2000 km as a function of mass fraction of COM from 0 to 50% and a leaching parameter between 0 and 90% (Fig. 4).

In the case of a body with a core of 500 km, close to those of Ceres, Dione, and the smallest dimension of Haumea's core, only a small volume fraction of the core (<40%) would have dehydrated even in the absence of leaching. For a 2,000 km core, close to the value for Titan and Ganymede, only 20–30% or the upper 200 km would remain below dehydration temperature in the absence of leaching, and it requires more than 50% of leaching to maintain a hydrated mineralogy in most of the core. Solutions compatible with the COM fractions (Fig. 2) and the MoI and mass are shown for Ganymede and Titan for 2000 km core radius, and for Ceres and Dione for 500 km core radius (Fig. 4).

The inferred COM content is high whatever the model of metamorphic evolution considered, although it is systematically

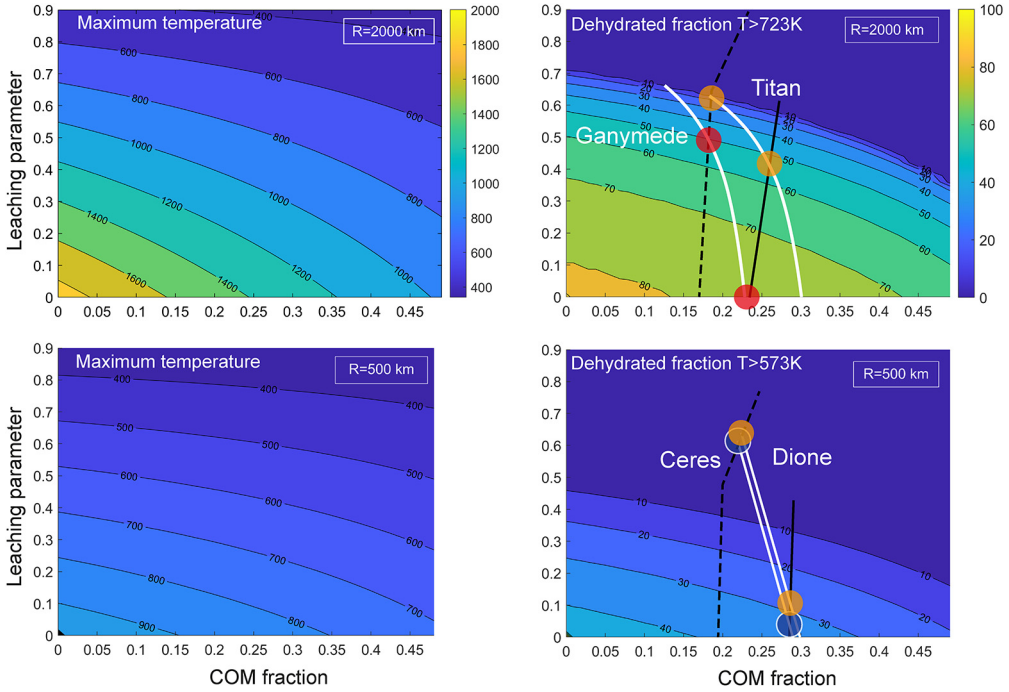

Fig. 4. Leaching parameter and COM mass fraction limit maximum temperature during thermal evolution of the core. Silicate dehydration temperature is taken halfway through the dehydration window. In small cores, thermal evolution models predict a small fraction of dehydrated core whatever the fractions of COM and leaching. In large cores, a larger range of silicate dehydration is obtained. White curves show parameters consistent with modeling of mass and MoI for Titan, Ganymede, Dione, and Ceres, and black lines parameters consistent with COM mass fraction evolution according to the pyrolysis and Vitrimat kinetic models (full and dashed lines, respectively). Solutions for each body are positioned at the intersection of the lines for extreme kinetics models.

lower by ∼5–10% for the Vitrimat model than for the pyrolysis model. The smaller fraction of dehydrated material in Titan than in Ganymede requires higher leaching parameter. The dehydrated fraction from thermal modeling for Ganymede is in the 50–80% range (Fig. 4), consistent with that from density model of 40–100% (Fig. 2). Values for Titan are 10–50% (Fig. 4) and 0–40% (Fig. 2), respectively. For both Ganymede and Titan, the extreme kinetic models yield limit values that are consistent between the density and thermal models. The actual densification of COM may also proceed at intermediate rates.

The thermal evolutions of Ceres and Dione are similar and point to small if any dehydration (Fig. 4). The dry silicate mineralogy inferred for Haumea using the pyrolysis model (Fig. 2b) is incompatible with the small dehydration inferred from thermal evolution. Thus either it was formed from dry silicates that underwent little interaction with water, or the evolution of the COM density is faster than inferred from the pyrolysis model, closer to that of the Vitrimat model, and consistent with little dehydration (Fig. 2d). Pressure is known to reduce the difference between graphitizing and non-graphitizing carbons and to favor densification (Beyssac et al., 2003), hence to reduce potential differences between the extreme models considered here. Kinetics of densification in these materials is not yet fully quantified, which calls for future experimental effort.

Although the amount of leaching is a poorly known parameter (Castillo-Rogez and Lunine, 2010), the present calculations show that a significant fraction of the core would remain at temperatures below that required for the complete pyrolysis of COM and dehydration of silicates during the whole evolution of an icy moon or dwarf planet. The maximum temperature and the volume fraction of the core that gets above silicate dehydration increase with increasing radius. With 25 wt% COM, the temperatures are still increasing at present day in cores with radius of at least 1000 km (Fig. S2), implying that silicate dehydration, carbonization of COM and associated volatile release may still be active on bodies like Pluto and larger. In cores of 500 km radius, temperature is now likely decreasing after reaching a maximum 1–2 Gyr after differentiation.

4. Implications for outer solar system objects

4.1. Bodies with constrained MoI and inner structure

The compositions of icy moons and dwarf planets can be reconciled with those of common precursors to CI chondrites and comets, reinforcing the idea that there is a continuum of bodies (Gounelle, 2011) formed in the outer solar system reservoir with large amounts of carbon and ice, distinct from volatile and carbon-poor planetary precursors of the inner solar system. The high COM content accounts for the ubiquity of organic and carbonaceous compounds at the surface of these bodies, whose origin could be largely endogenous due to pyrolysis of the original IOM during metamorphism.

Icy moons and dwarf planets have an atomic C/Si ratio ($3 < C/Si < 6$) intermediate between that of carbonaceous chondrites ($C/Si < 0.8$) and that of comets ($C/Si \sim 17$), and close to that of the Sun (7.08). Their current composition likely derives from precursors in solar proportion, carbon loss during thermal evolution explaining the slight depletion with respect to the Sun. They could thus have formed by homogeneous accretion of solar mixture of components, causing extensive silicate hydration prior to ice-core differentiation. The C/Si ratio of UCAMM, of proposed cometary origin (Dartois et al., 2013), is even higher than in comets. It is consistent with COM in CI-IDP-UCAMM having formed by irradiation of nebular organic molecules trapped at the surface or inside ice grains (Dartois et al., 2013; Laurent et al., 2015), and concur with the hypothesis of a SSC-free “cometary” component (Fig. 1) formed by IOM beyond the “soot line” and mixed with ices formed beyond the snow line.

Moderate temperatures of Titan core are favored by the large COM fraction, and require substantial leaching of radioactive

elements (Fig. 4). Larger leaching parameter in Titan than in Ganymede is possibly explained by a delay in ice-core differentiation in Titan of 0.5–1.5 Gyr with respect to Ganymede as estimated from equation (7), by stronger water-rock interactions in Titan than Ganymede, and by metallic inner core differentiation in Ganymede. Similar delays of differentiation in Titan were inferred from numerical simulations (O'Rourke and Stevenson, 2014). Heterogeneous accretion of refractory compounds (SSC and COM) and ice may be needed to explain Ganymede's core density and essentially dry silicate mineralogy that requires little interaction between ice and water when the pyrolysis model is used (Fig. 2a), a condition that is lifted if the Vitrimat model allowing for more hydrated mineralogy is used (Fig. 2c). Europa's dry silicate mineralogy and high temperature of COM metamorphism and its small ice/core ratio are consistent with heterogeneous accretion, in line with proposed formation in the vicinity of the snow line in Jupiter's nebula for Europa (Ronnet et al., 2017). With its high-carbon low-water content, Europa could actually have formed mostly between the "snow" and "soot" lines of the Jovian nebula. Central temperatures above the eutectic melting point in the Fe-FeS system (Fei et al., 1997) are consistent with small (~6 wt%) metallic inner core (Sohl et al., 2002) assuming eutectic composition and density of 5700 kg/m^3 (Morard et al., 2018), and imply that only about 25% of Europa's core differentiated to form an inner metallic core. For Ganymede, magnetic data also support the existence of a small inner metallic core (Kivelson et al., 2002). Even though maximum temperatures are high, COM may be largely preserved in the form of coal or graphitic material in the outer regions of Ganymede's and Europa's core. In large moons, the effects of pressure on COM density should also be investigated in order to restrain the possible compositional models. Densification of COM analogs should be studied at high-pressure for comparison with coal-like materials (Beyssac et al., 2003; Le Bayon et al., 2012; Nakamura et al., 2020).

Coexistence of large undifferentiated outer core layer and minor (25%) differentiated layer above an inner metallic core is possible owing to the similar bulk densities of SSC component, of 3750 and 3800 kg/m^3, respectively. Ganymede's outer and inner cores may have a similar nature to Europa, the size of the inner metallic core of Ganymede inferred from magnetic data is not well constrained (Kivelson et al., 2002), and hydration of part of its outer core is also possible (Néri et al., 2020). Refinements of the inner density and thermal structures of Callisto, Ganymede and Europa will await the more accurate gravimetric and magnetic data from the JUICE and Europa Clipper missions. Slowly heating COM-rich outer core layers may still be releasing complex organics to the icy layers and ocean.

Thermal models in Dione and Ceres match temperature windows defined by mineralogy and COM density for a leaching parameter in the range 0–0.5 (Fig. 4). For Haumea, the small (<40%) dehydration inferred from thermal models (Fig. 4) is inconsistent with that inferred if the densification of COM is given by the pyrolysis model (Fig. 2a), and consistent with that inferred from the Vitrimat model (Fig. 2c), a range of intermediate solutions being satisfactory. Low ice/refractory ratio was attributed to erosion by an impact after differentiation causing its present high rotation speed and elongated shape (Dunham et al., 2019), but the position of Haumea on the CI-Solar continuum (Fig. 1) suggests it may be inherited from formation in a SSC-rich environment. Ceres also has low ice content. Ceres is thought to have formed in the outer solar system (De Sanctis et al., 2015) and to have migrated to the asteroid belt early in the solar system history. Ceres is now subjected to high enough temperatures for ice to sublimate, but its relatively old surface argues against large-scale sublimation. Low ice/refractory ratio is thus likely a feature inherited from formation, potentially near the snow line.

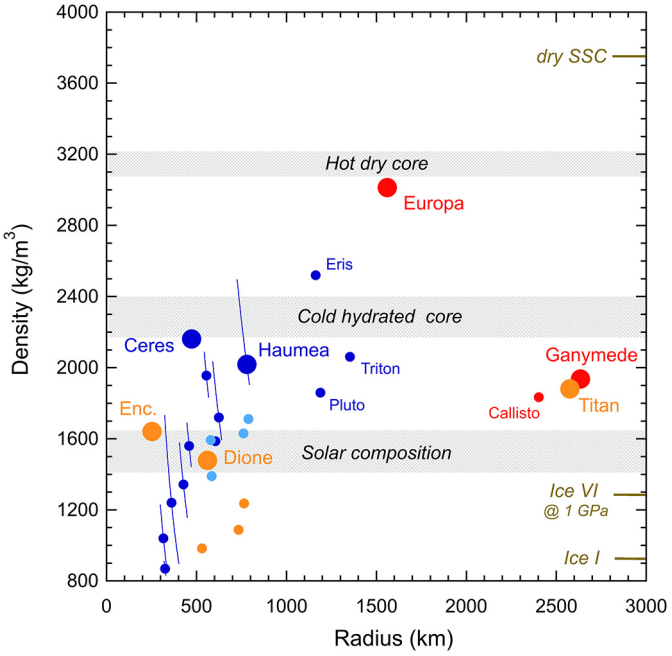

Fig. 5. Bulk density of outer solar system objects as a function of radius. Densities calculated for solar composition and hydrated refractory core bracket the densities of most large icy outer solar system objects, at the exception of Europa and Eris whose large densities requires small ice content and dry SSC mineralogies. Large symbols are used for bodies with known moment of inertia. Dwarf planets and trans-Neptunian objects in dark blue symbols (Braga-Ribas et al., 2013; Brown, 2013; Dunham et al., 2019; Grundy et al., 2019; Kiss et al., 2019; Malamud and Prialnik, 2015; Sicardy et al., 2011). Triton, captured by Neptune, is ascribed to the same family. Same color code as Fig. 1, and light blue for Uranus moons. Densities of ices and dry SSC are indicated. The effect of pressure on bulk density is about 15% between Enceladus and Titan, largely due to compression and stabilization of ice VI in the hydrosphere. At small radii, low densities correspond to ice-rich bodies. Porosity is unlikely in bodies close to hydrostatic equilibrium (large symbols) and large bodies (R > 500 km). Values are given in Table 2.

4.2. Consequences for other moons and dwarf planets

Bulk densities of Ganymede, Titan, and Dione, for which internal structure and carbon-rich composition is inferred, are bracketed by the densities of the solar composition and its refractory part with hydrous silicate mineralogy (Fig. 5). Jupiter's moon Callisto, Uranus moons (Titania, Oberon, Umbriel, Ariel), and Pluto, Charon, Triton, as well as several other dwarf planets (2007 OR$_{10}$, Quaoar, Orcus) have similar bulk densities, supporting the idea that their refractory cores are composed of a mixture of CI chondrite and COM. This is consistent with large carbonaceous matter contents and hydrous mineralogy assumed in modeling of the density of the Pluto-Charon system (McKinnon et al., 2017), and with the idea of a primordial composition with density of ~1800 kg/m^3 for dwarf planets (Barr and Schwamb, 2016).

The present thermal models show that totally dry silicate mineralogy cannot be formed by dehydration of originally hydrated silicates by internal heating alone in bodies with core radius below 1000 km (Fig. 4). Dry silicate mineralogy and low ice/core ratios are possible for Haumea (Fig. 2b) and certain for Eris (Fig. 5), features they share with Europa and likely inherited from their formation. These characteristics were used to propose that Europa formed in the vicinity of the snow line in Jupiter's nebula (Ronnet et al., 2017). Eris, and possibly Haumea, may thus have formed partly between the "soot" and "snow" lines in the early solar nebula, although they are currently further than 40 AU from the Sun. The snow line can lie as far as 20 AU at early stages of nebular evolution in models where carbon is mostly in a condensed carbonaceous form (Min et al., 2011), and even beyond if observations

of the snow line being further than Neptune's orbit equivalent in the V883 Ori nebula (Cieza et al., 2016) reflect conditions in the early solar nebula. Low ice/refractory ratios and dry silicate mineralogy may thus be primary features of carbon-rich dwarf planets forming in a solar nebula with carbon mostly in the form of carbonaceous matter.

A third group of bodies present densities that are below that of the solar composition of 1400 ± 70 kg/m^3. Since many of these have radii lower than 400 km, porosity may exist due to low internal pressure and contribute to lowering the density. Saturn's moons Rhea, Iapetus, and Tethys have low density and larger than 400 km radii that make high porosities unlikely, suggesting they have a low SSC component and high ice content requiring specific timing or mode of formation that remain to be investigated.

4.3. Implications for planetary modeling and observations

The extraction of the volatile and light liquid hydrocarbons released during pyrolysis of COM may contribute to forming insulating hydrate layers on Pluto (Kamata et al., 2019) or thick atmosphere on Titan (Miller et al., 2019). This process may be reflected in the variety of compounds ranging from volatile, e.g. nitrogen and light hydrocarbons in Titan's atmosphere (Miller et al., 2019), to macromolecular carbon in Enceladus plumes (Postberg et al., 2018) that reach the surface of icy moons and dwarf planets through cryovolcanism and hydrothermal activity. Modeling the complex interactions between gaseous species and ices or atmospheres is out of the goal of the present study, and must be tailored to each body. Also, there is a dearth of laboratory data on the interaction between SSC and COM in the range 500–1000 K where both dehydration and carbonization occur (Néri et al., 2020).

With temperatures still increasing at present time in carbon-rich cores larger than 1000 km (Fig. S2), active dehydration and release of organics from the core may be sustained to present-day, providing fluids that can fuel hydrothermal activity on intermediate-size bodies such as Europa, Eris, Triton, and Pluto. Dark geysers observed on Triton, a likely dwarf planet captured by Neptune, are also believed to derive from nitrogen-hydrocarbon mixtures (Soderblom et al., 1990), as well as the different materials (dark organic matter, red tholins and nitrogen ice) at the surface of Pluto and Charon (Grundy et al., 2016), and of Ceres (Marchi et al., 2019). These observations support the idea that COM is degrading at present day in the core of icy moons and dwarf planets.

Among dwarf planets, first estimate of the density of Haumea lead to a value of ~2550 kg/m^3 that has since been refined to ~2020 kg/m^3. Current measurements of the shape of Haumea (radius ~800 km) are precise enough to refine parameters of the Jacobi ellipsoid and its internal density structure (Dunham et al., 2019), giving an estimated carbon content of 14% (Table 2). For Quaoar, occultation measurements are best fitted with a McLaurin ellipsoid shape of average radius of ~600 km, flattening coefficient of $0.087^{+0.027/-0.018}$, and a density of 1990 ± 460 kg/m^3 (Braga-Ribas et al., 2013). A model of Quaoar using the present solar composition density and assuming ice-core differentiation gives a flattening coefficient of 0.077, whereas assuming a homogeneous body yields 0.09. The two hypotheses are thus unresolved within current uncertainties. For Quaoar and bodies like 2007 UK_{126} (Grundy et al., 2019) whose size is close to that of Dione, repeated and more precise measurements may yield resolvable inner structures within the coming years. The proliferation of stellar occultation networks and observations by the James Webb Space Telescope will improve our knowledge of the shape and composition of the TNOs in the coming decade, and provide insights on the abundance of COM in these objects. For smaller bodies like 2003 UZ_{413} (radius ~300 km close to that of Enceladus), relative uncertainties are even higher and whether precise enough measurements may be obtained from current telescopes is to be tested.

The carbon-rich composition of icy moons and dwarf planets confirms that condensed organic carbon is a major component of bodies forming beyond the "soot" and "snow" lines in the primitive solar system. Carbon should thus be considered in modeling the composition and density of exoplanets that formed near and beyond the snow line before migrating towards their stars, in particular the low densities of Earth-sized to super-Earth exoplanets (Delrez et al., 2021; Gillon et al., 2017; Luque and Pallé, 2022). Formation of inner Jovian moons like Europa with high-carbon low-water contents supports carbon-rich models for Jupiter (Lodders, 2004). Carbon-rich Jupiter-like models are consistent with the observation of hydrocarbons in the haze that surround hot giant exoplanets (Gao et al., 2020). Thus extrasolar carbon-planets could be common, which has implications on their habitability potential.

CRediT authorship contribution statement

Authors contributed equally to the article.

Declaration of competing interest

The authors declare that they have no known competing financial interests or personal relationships that could have appeared to influence the work reported in this paper.

Data availability

Data will be made available on request.

Acknowledgements

This work was supported by Institut National des Sciences de l'Univers through Programme National de Planétologie. BR acknowledges the LABEX Lyon Institute of Origins (ANR-10-LABX-0066) Lyon for its financial support within the Plan France 2030 of the French government operated by the National Research Agency (ANR). CS acknowledges the support of NASA's 'Exploring Ocean Worlds' Research Coordinated Network (award 80NSSC19K1427), managed by the Woods Hole Oceanographic Institution. This work has been co-funded by the European Union (ERC, PROMISES, project #101054470). Views and opinions expressed are however those of the authors only and do not necessarily reflect those of the European Union or the European Research Council. Neither the European Union nor the granting authority can be held responsible for them. Thoughtful comments from two anonymous reviewers helped improve the manuscript.

Appendix A. Supplementary material

Supplementary material related to this article can be found online at https://doi.org/10.1016/j.epsl.2023.118172.

References

Alexander, C.M.O.D., Fogel, M., Yabuta, H., Cody, G.D., 2007. The origin and evolution of chondrites recorded in the elemental and isotopic compositions of their macromolecular organic matter. Geochim. Cosmochim. Acta 71, 4380–4403. https://doi.org/10.1016/j.gca.2007.06.052.

Bardyn, A., Baklouti, D., Cottin, H., Fray, N., Briois, C., et al., 2017. Carbon-rich dust in comet 67P/Churyumov-Gerasimenko measured by COSIMA/Rosetta. Mon. Not. R. Astron. Soc. 469, S712–S722. https://doi.org/10.1093/mnras/stx2640.

Barr, A.C., Schwamb, M.E., 2016. Interpreting the densities of the Kuiper belt's dwarf planets. Mon. Not. R. Astron. Soc. 460, 1542–1548. https://doi.org/10.1093/mnras/stw1052.

Beyssac, O., Brunet, F., Petitet, J.-P., Goffé, B., Rouzaud, J.-N.e., 2003. Experimental study of the microtextural and structural transformations of carbonaceous materials under pressure and temperature. Eur. J. Mineral. 15, 937–951. https://doi.org/10.1127/0935-1221/2003/0015-0937.

Beyssac, O., Goffé, B., Chopin, C., Rouzaud, J.N., 2002. Raman spectra of carbonaceous material in metasediments: a new geothermometer. J. Metamorph. Geol. 20, 859–871. https://doi.org/10.1046/j.1525-1314.2002.00408.x.

Braga-Ribas, F., Sicardy, B., Ortiz, J.L., Lellouch, E., Tancredi, G., et al., 2013. The size, shape, albedo, density, and atmospheric limit of TransNeptunian object (50000) Quaoar from multichord stellar occultations. Astrophys. J. 773, 26. https://doi.org/10.1088/0004-637x/773/1/26.

Brown, M.E., 2013. The density of mid-sized Kuiper belt object 2002 UX25 and the formation of dwarf planets. Astrophys. J. 778, L34. https://doi.org/10.1088/2041-8205/778/2/l34.

Burnham, A.K., 2019. Kinetic models of vitrinite, kerogen, and bitumen reflectance. Org. Geochem. 131, 50–59. https://doi.org/10.1016/j.orggeochem.2019.03.007.

Carslaw, H., Jaeger, J., 1959. Conduction of Heat in Solids, 2nd ed. Clarendon, London.

Castillo-Rogez, J.C., Lunine, J.I., 2010. Evolution of Titan's rocky core constrained by Cassini observations. Geophys. Res. Lett. 37, L20205. https://doi.org/10.1029/2010GL044398.

Cieza, L.A., Casassus, S., Tobin, J., Bos, S.P., Williams, J.P., et al., 2016. Imaging the water snow-line during a protostellar outburst. Nature 535, 258–261. https://doi.org/10.1038/nature18612.

Clauser, C., Huenges, E., 1995. Thermal conductivity of rocks and minerals. In: Ahrens, T.J. (Ed.), Rocks Physics and Phase Relations: A Handbook of Physical Constants. American Geophysical Union, Washington D.C., pp. 105–126.

Connolly, J.A.D., 1990. Multivariable phase diagrams; an algorithm based on generalized thermodynamics. Am. J. Sci. 290, 666–718. https://doi.org/10.2475/ajs.290.6.666.

Dartois, E., Engrand, C., Brunetto, R., Duprat, J., Pino, T., et al., 2013. UltraCarbonaceous Antarctic micrometeorites, probing the Solar System beyond the nitrogen snow-line. Icarus 224, 243–252. https://doi.org/10.1016/j.icarus.2013.03.002.

De Sanctis, M.C., Ammannito, E., Raponi, A., Marchi, S., McCord, T.B., et al., 2015. Ammoniated phyllosilicates with a likely outer Solar System origin on (1) Ceres. Nature 528, 241–244. https://doi.org/10.1038/nature16172.

Delrez, L., Ehrenreich, D., Alibert, Y., Bonfanti, A., Borsato, L., et al., 2021. Transit detection of the long-period volatile-rich super-Earth ν^2 Lupi d with CHEOPS. Nat. Astron. 5, 775–787. https://doi.org/10.1038/s41550-021-01381-5.

Dunham, E.T., Desch, S.J., Probst, L., 2019. Haumea's shape, composition, and internal structure. Astrophys. J. 877, 41. https://doi.org/10.3847/1538-4357/ab13b3.

Ermakov, A.I., Fu, R.R., Castillo-Rogez, J.C., Raymond, C.A., Park, R.S., et al., 2017. Constraints on Ceres' internal structure and evolution from its shape and gravity measured by the dawn spacecraft. J. Geophys. Res., Planets 122, 2267–2293. https://doi.org/10.1002/2017JE005302.

Fei, Y., Bertka, C.M., Finger, L.W., 1997. High-pressure iron-sulfur compound, Fe3S2, and melting relations in the Fe-FeS system. Science 275, 1621–1623. https://doi.org/10.1126/science.275.5306.1621.

Fortes, A.D., 2012. Titan's internal structure and the evolutionary consequences. Planet. Space Sci. 60, 10–17. https://doi.org/10.1016/j.pss.2011.04.010.

Franklin, R.E., 1949. A study of the fine structure of carbonaceous solids by measurements of true and apparent densities. Part II.—Carbonized coals. Trans. Faraday Soc. 45, 668–682. https://doi.org/10.1039/TF9494500668.

Franklin, R.E., Randall, J.T., 1951. Crystallite growth in graphitizing and non-graphitizing carbons. Proc. R. Soc. Lond. Ser. A, Math. Phys. Sci. 209, 196–218. https://doi.org/10.1098/rspa.1951.0197.

Ganino, C., Libourel, G., 2017. Reduced and unstratified crust in CV chondrite parent body. Nat. Commun. 8, 261. https://doi.org/10.1038/s41467-017-00293-1.

Gao, P., Thorngren, D.P., Lee, G.K.H., Fortney, J.J., Morley, C.V., et al., 2020. Aerosol composition of hot giant exoplanets dominated by silicates and hydrocarbon hazes. Nat. Astron. 4, 951–956. https://doi.org/10.1038/s41550-020-1114-3.

Gillon, M., Triaud, A.H.M.J., Demory, B.-O., Jehin, E., Agol, E., et al., 2017. Seven temperate terrestrial planets around the nearby ultracool dwarf star TRAPPIST-1. Nature 542, 456–460. https://doi.org/10.1038/nature21360.

Gounelle, M., 2011. The asteroid–comet continuum: in search of lost primitivity. Elements 7, 29–34. https://doi.org/10.2113/gselements.7.1.29.

Grundy, W.M., Binzel, R.P., Buratti, B.J., Cook, J.C., Cruikshank, D.P., et al., 2016. Surface compositions across Pluto and Charon. Science 351, aad9189. https://doi.org/10.1126/science.aad9189.

Grundy, W.M., Noll, K.S., Buie, M.W., Benecchi, S.D., Ragozzine, D., et al., 2019. The mutual orbit, mass, and density of transneptunian binary G!kún‖'hòmdímà (229762 2007 UK_{126}). Icarus 334, 30–38. https://doi.org/10.1016/j.icarus.2018.12.037.

Hemingway, D., Iess, L., Tajeddine, R., Tobie, G., 2018. The interior of Enceladus. In: Schenk, P., Clark, R., Howette, C., Verbiscer, A.J., Waite, J. (Eds.), Enceladus and the Icy Moons of Saturn. The University of Arizona Press, Tucson, pp. 57–77.

Herrin, J.M., Deming, D., 1996. Thermal conductivity of U.S. coals. J. Geophys. Res., Solid Earth 101, 25381–25386. https://doi.org/10.1029/96JB01884.

Iess, L., Jacobson, R.A., Ducci, M., Stevenson, D.J., Lunine, J.I., et al., 2012. The tides of Titan. Science 337, 457–459. https://doi.org/10.1126/science.1219631.

Jessberger, E.K., Christoforidis, A., Kissel, J., 1988. Aspects of the major element composition of Halley's dust. Nature 332, 691–695. https://doi.org/10.1038/332691a0.

Kamata, S., Nimmo, F., Sekine, Y., Kuramoto, K., Noguchi, N., et al., 2019. Pluto's ocean is capped and insulated by gas hydrates. Nat. Geosci. 12, 407–410. https://doi.org/10.1038/s41561-019-0369-8.

Kiss, C., Marton, G., Parker, A.H., Grundy, W.M., Farkas-Takács, A., et al., 2019. The mass and density of the dwarf planet (225088) 2007 OR10. Icarus 334, 3–10. https://doi.org/10.1016/j.icarus.2019.03.013.

Kivelson, M.G., Khurana, K.K., Volwerk, M., 2002. The permanent and inductive magnetic moments of ganymede. Icarus 157, 507–522. https://doi.org/10.1006/icar.2002.6834.

Kress, M.E., Tielens, A.G.G.M., Frenklach, M., 2010. The 'soot line': destruction of presolar polycyclic aromatic hydrocarbons in the terrestrial planet-forming region of disks. Adv. Space Res. 46, 44–49. https://doi.org/10.1016/j.asr.2010.02.004.

Laurent, B., Roskosz, M., Remusat, L., Robert, F., Leroux, H., et al., 2015. The deuterium/hydrogen distribution in chondritic organic matter attests to early ionizing irradiation. Nat. Commun. 6, 8567. https://doi.org/10.1038/ncomms9567.

Le Bayon, R., Adam, C., Ferreiro Mählmann, R., 2012. Experimentally determined pressure effect on vitrinite reflectance at 450 °C. Int. J. Coal Geol. 92, 69–81. https://doi.org/10.1016/j.coal.2011.12.007.

Lee, J.-E., Lee, S., Baek, G., Aikawa, Y., Cieza, L., et al., 2019. The ice composition in the disk around V883 Ori revealed by its stellar outburst. Nat. Astron. 3, 314–319. https://doi.org/10.1038/s41550-018-0680-0.

Lodders, K., 2003. Solar system abundances and condensation temperatures of the elements. Astrophys. J. 591, 1220–1247. https://doi.org/10.1086/375492.

Lodders, K., 2004. Jupiter formed with more tar than ice. Astrophys. J. 611, 587–597. https://doi.org/10.1086/421970.

Luque, R., Pallé, E., 2022. Density, not radius, separates rocky and water-rich small planets orbiting M dwarf stars. Science 377, 1211–1214. https://doi.org/10.1126/science.abl7164.

Macke, R.J., Consolmagno, G.J., Britt, D.T., 2011. Density, porosity, and magnetic susceptibility of carbonaceous chondrites. Meteorit. Planet. Sci. 46, 1842–1862. https://doi.org/10.1111/j.1945-5100.2011.01298.x.

Malamud, U., Prialnik, D., 2015. Modeling Kuiper belt objects Charon, Orcus and Salacia by means of a new equation of state for porous icy bodies. Icarus 246, 21–36. https://doi.org/10.1016/j.icarus.2014.02.027.

Mao, X., McKinnon, W.B., 2018. Faster paleospin and deep-seated uncompensated mass as possible explanations for Ceres' present-day shape and gravity. Icarus 299, 430–442. https://doi.org/10.1016/j.icarus.2017.08.033.

Marchi, S., Raponi, A., Prettyman, T.H., De Sanctis, M.C., Castillo-Rogez, J., et al., 2019. An aqueously altered carbon-rich Ceres. Nat. Astron. 3, 140–145. https://doi.org/10.1038/s41550-018-0656-0.

Martins, Z., Chan, Q.H.S., Bonal, L., King, A., Yabuta, H., 2020. Organic matter in the solar system—implications for future on-site and sample return missions. Space Sci. Rev. 216, 54. https://doi.org/10.1007/s11214-020-00679-6.

McKinnon, W.B., 2015. Effect of Enceladus's rapid synchronous spin on interpretation of Cassini gravity. Geophys. Res. Lett. 42, 2137–2143. https://doi.org/10.1002/2015GL063384.

McKinnon, W.B., Stern, S.A., Weaver, H.A., Nimmo, F., Bierson, C.J., et al., 2017. Origin of the Pluto–Charon system: constraints from the new horizons flyby. Icarus 287, 2–11.

Miller, K.E., Glein, C.R., Waite, J.H., 2019. Contributions from accreted organics to Titan's atmosphere: new insights from cometary and chondritic data. Astrophys. J. 871, 59. https://doi.org/10.3847/1538-4357/aaf561.

Min, M., Dullemond, C.P., Kama, M., Dominik, C., 2011. The thermal structure and the location of the snow line in the protosolar nebula: axisymmetric models with full 3-D radiative transfer. Icarus 212, 416–426. https://doi.org/10.1016/j.icarus.2010.12.002.

Morard, G., Bouchet, J., Rivoldini, A., Antonangeli, D., Roberge, M., et al., 2018. Liquid properties in the Fe-FeS system under moderate pressure: Tool box to model small planetary cores. Am. Mineral. 103, 1770–1779. https://doi.org/10.2138/am-2018-6405.

Nakamura, Y., Yoshino, T., Satish-Kumar, M., 2020. Pressure dependence of graphitization: implications for rapid recrystallization of carbonaceous material in a subduction zone. Contrib. Mineral. Petrol. 175, 32. https://doi.org/10.1007/s00410-020-1667-2.

Néri, A., Guyot, F., Reynard, B., Sotin, C., 2020. A carbonaceous chondrite and cometary origin for icy moons of Jupiter and Saturn. Earth Planet. Sci. Lett. 530, 115920. https://doi.org/10.1016/j.epsl.2019.115920.

O'Rourke, J., Stevenson, D., 2014. Stability of ice/rock mixtures with application to a partially differentiated Titan. Icarus 227, 67–77. https://doi.org/10.1016/j.icarus.2013.09.010.

Okumura, F., Mimura, K., 2011. Gradual and stepwise pyrolyses of insoluble organic matter from the Murchison meteorite revealing chemical structure and isotopic distribution. Geochim. Cosmochim. Acta 75, 7063–7080. https://doi.org/10.1016/j.gca.2011.09.015.

Osako, M., Yoneda, A., Ito, E., 2010. Thermal diffusivity, thermal conductivity and heat capacity of serpentine (antigorite) under high pressure. Phys. Earth Planet. Inter. 183, 229–233. https://doi.org/10.1016/j.pepi.2010.07.005.

Pizzarello, S., Cooper, G., Flynn, G.J., 2006. The Nature and Distribution of the Organic Material in Carbonaceous Chondrites and Interplanetary Dust Particles.

Postberg, F., Khawaja, N., Abel, B., Choblet, G., Glein, C.R., et al., 2018. Macromolecular organic compounds from the depths of Enceladus. Nature 558, 564–568. https://doi.org/10.1038/s41586-018-0246-4.

Ronnet, T., Mousis, O., Vernazza, P., 2017. Pebble accretion at the origin of water in europa. Astrophys. J. 845, 92. https://doi.org/10.3847/1538-4357/aa80e6.

Rotundi, A., Sierks, H., Della Corte, V., Fulle, M., Gutierrez Pedro, J., et al., 2015. Dust measurements in the coma of comet 67P/Churyumov-Gerasimenko inbound to the Sun. Science 347, aaa3905. https://doi.org/10.1126/science.aaa3905.

Sicardy, B., Ortiz, J.L., Assafin, M., Jehin, E., Maury, A., et al., 2011. A Pluto-like radius and a high albedo for the dwarf planet Eris from an occultation. Nature 478, 493–496. https://doi.org/10.1038/nature10550.

Soderblom, L.A., Kieffer, S.W., Becker, T.L., Brown, R.H., Cook, A.F., et al., 1990. Triton's Geyser-like plumes: discovery and basic characterization. Science 250, 410. https://doi.org/10.1126/science.250.4979.410.

Sohl, F., Spohn, T., Breuer, D., Nagel, K., 2002. Implications from Galileo observations on the interior structure and chemistry of the Galilean satellites. Icarus 157, 104–119. https://doi.org/10.1006/icar.2002.6828.

Vance, S., Bouffard, M., Choukroun, M., Sotin, C., 2014. Ganymede's internal structure including thermodynamics of magnesium sulfate oceans in contact with ice. Planet. Space Sci. 96, 62–70. https://doi.org/10.1016/j.pss.2014.03.011.

Wasson, J.T., Kallemeyn, G.W., 1988. Composition of chondrites. Philos. Trans. R. Soc. Lond. Ser. A, Math. Phys. Sci. 325, 535–544.

Yokoyama, T., Nagashima, K., Nakai, I., Young, E.D., Abe, Y., et al., 2022. Samples returned from the asteroid Ryugu are similar to Ivuna-type carbonaceous meteorites. Science 379, eabn7850. https://doi.org/10.1126/science.abn7850.

Zandanel, A., Hellmann, R., Truche, L., Roddatis, V., Mermoux, M., et al., 2022. Geologically rapid aqueous mineral alteration at subfreezing temperatures in icy worlds. Nat. Astron. 6, 554–559. https://doi.org/10.1038/s41550-022-01613-2.

Zannoni, M., Hemingway, D., Gomez Casajus, L., Tortora, P., 2020. The gravity field and interior structure of Dione. Icarus 345, 113713. https://doi.org/10.1016/j.icarus.2020.113713.

Zolotov, M.Y., 2020. The composition and structure of Ceres' interior. Icarus 335, 113404. https://doi.org/10.1016/j.icarus.2019.113404.